Development of Brain Targeting Peptide Based MMP-9 Inhibiting Nanoparticles for the Treatment of Brain Diseases with Elevated MMP-9 Activity

Yamir Islam,[1] Aneesa Khalid,[1] Stefano Pluchino,[2] Muttuswamy Sivakumaran,[3] Meritxell Teixidò,[4] Andrew Leach,[1,b] Amos A. Fatokun,[1] James Downing,[1] Christopher Coxon,[1,a] Touraj Ehtezazi,[1]*

[1]School of Pharmacy and Biomolecular Sciences, Liverpool John Moores University, Liverpool, L3 3AF, UK

[2]Department of Clinical Neurosciences, Clifford Allbutt Building - Cambridge Biosciences Campus and NIHR Biomedical Research Centre, University of Cambridge, Hills Road, CB2 0HA Cambridge, UK.

[3]Department of Haematology, Peterborough City Hospital, Edith Cavell Campus, Bretton Gate Peterborough, PE3 9GZ, Peterborough, UK.

[4]Institute for Research in Biomedicine (IRB Barcelona), Barcelona Institute of Science and Technology (BIST), Baldiri Reixac 10, Barcelona 08028, Spain.

[a]current address: Institute of Chemical Sciences, School of Engineering and Physical Sciences, Heriot-Watt University, Edinburgh, EH14 4AS

[b]current address: School of Pharmacy,University of Manchester, Manchester, UK

*Corresponding Author: t.ehtezazi@ljmu.ac.uk

Abstract

Latent and active levels of cerebral matrix metalloproteinase 9 (MMP-9) are elevated in neurological diseases and brain injuries, contributing to neurological damage and poor clinical outcomes. This study aimed developing peptide-based nanoparticles with ability to cross the blood-brain-barrier (BBB) and inhibit MMP-9.

Three amphiphilic peptides were synthesised containing brain-targeting ligands (HAIYPRH or CKAPETALC) conjugated with MMP-9 inhibiting peptide (CTTHWGFTLC) linked by glycine (spacer) at the N-terminus, and the peptide sequences were conjugated at the N-terminus to cholesterol. ^{19}F-NMR assay was developed to measure MMP-9 inhibition. Cell toxicity was evaluated by the LDH assay, and dialysis studies were conducted with/without fetal bovine serum. An *in vitro* model was employed to evaluate the ability of nanoparticles crossing the BBB.

The amphiphilic peptide (Cholesterol-GGGCTTHWGFTLCHAIYPRH) formed nanoparticles (average size of 202.8 nm) with ability to cross the BBB model. MMP-9 inhibiting nanoparticles were non-toxic to cells, and reduced MMP-9 activity from k_{obs} of $4.5\times10^{-6}s^{-1}$ to complete inhibition. Dialysis studies showed that nanoparticles did not disassemble by extreme dilution (40 folds), but gradually hydrolysed by serum enzymes.

In conclusion, the MMP-9 inhibiting nanoparticles reduced the activity of MMP-9, with acceptable serum stability, minimal cell toxicity and ability to cross the *in vitro* BBB model.

Keywords: MMP-9 inhibitor, nanoparticles, brain drug delivery, blood-brain-barrier

1. Introduction

The matrix metalloproteinases (MMPs) belonging to the metzincin family.[1] In humans, 23 different MMPs have been discovered[2] and are divided into soluble-type MMPs and membrane bound MMPs.[3] MMPs are sub-grouped into collagenases, gelatinases, stromelysins and matrilysins.[4] Collectively MMPs metabolize extracellular matrix. [1,3,5]

Matrix metalloproteinase 9 (MMP-9) or gelatinase B is a member of large MMPs family. MMP-9 not only metabolize the denatured collagen[6] but also breakdown various collagens, activate and modify cytokine and chemokines.[7] MMP-9 is expressed in the CNS as well as the peripheral nervous systems. MMP-9 expression is elevated in neurological diseases such as traumatic brain injury,[8] and multiple sclerosis (MS);[9] and its high levels are believed to be associated with poor outcomes.[8] Kumari *et al* 2011 showed that the proteolytic activity of MMP-9 was significantly increased in the ipsilateral hemispheres of *db/db* mice compared to *db/+* mice and this increased the chance of infarction in *db/db* mice.[10] MMP-9 expression correlated with stroke severity and poor outcome, and clinical trials were recommended testing agents antagonizing MMP-9 effects.[11]

Various efforts have been made to develop inhibitors for MMP-9 partially or completely. For example, Nyormoi et al. 2003 have reported an inhibtor of MMP-9 (compound 5a), that has antineoplastic activity. Furthermore, They reported that compound 5a did not act directly on mitochondia but it exhibits antineoplastic activity by ligand-receptor interaction and caspase 8 activation.[12] As another example, racemic ND-336, a selective MMP-9 inhibitor has demonstrated higher healing ability compared to becaplermin as MMP-9 promotes the damaging effects in diabetic foot ulcers.[13] Several MMP-9 inhibitors have been reported such as GS-5745,[14] and AQU-118, [15] but there is still need to identify an inhibitor with opimum activity and less toxicity. To achieve this target, MMP-9-siRNA was conjugated to quantum dots with a size of 15 nm. The aim was to downregulate MMP-9 expression in brain

microvascular endothelial cells.[16] To use a magnetic platform to guide nanoparticles (NPs) to the brain, tissue inhibitor of matrix metalloproteinases 1 (TIMP-1), an endogenous inhibitor of matrix metalloproteinases, was surface adsorbed on magnetic NPs (size of 10 nm). In the presence of static magnet, the NPs crossed human *in vitro* blood-brain-barrier (BBB) model.[17]

In another study, TIMP-1 loaded poly(lactic-co-glycolic acid) (PLGA) NPs were developed to enhance delivery of TIMP-1 to the brain. The NPs coated with polysorbate 80 (PS80) and penetrated the BBB following intravenous injections into mice.[18] On the other hand in another work, PLGA NPs (260 nm) were coated with PS80, which contained β-carotene (to reduce oxidative stress in organs). After intravenous administration, the majority of these NPs were observed to accumulate in the lungs rather than the brains of rats (2000 nmol/g in lungs compared to 0.2 nmol/g in the brain).[19] This study shows that NPs should be decorated with brain targeting ligands for the treatment of brain diseases.[20] Furthermore, Chen *et al* found that associated adeno virus (AAV) presenting an epitope of WPFYGTP showed 35 times greater efficiency in targeting the brain than the liver. Interestingly, AAVs with epitopes for brain microvessels of wild-type mice were not effective for mucopolysaccharidosis type VII mouse brain.[20] Therefore, brain targeting ligands may be suitable for certain diseases, but not for others. Hence, the brain targeting ligand should be chosen in relation to the brain disease. Although the above approaches are effective methods to inhibit MMP-9 in brain diseases, there is a need for nanoparticles that can be administered intravenously with specifically targeting the brain to inhibit MMP-9 for a few hours, but that are degraded by the brain/systemically. This is because, human studies indicated that the useful therapeutic window for MMP-9 inhibition is up to 72 h postinjury in traumatic brain injury.[21] It is believed that MMPs such as MMP-9 cause detrimental effects during early ischemic phase, but they are beneficial for reestablishment of cerebral blood flow and angiogenesis.[22-25]

Minocycline with MMP-9 inhibiting property[26] has been used in clinical trials with success for the treatment of stroke.[27] However, as high doses are required (10 mg/kg), and the toxicity of the drug has been fatal for some patients.[27] Another recent clinical trial showed the benefits of using minocycline (200 mg/day) for 6 months in patients to prevent the risk of conversion from clinically isolated demyelinating syndrome to multiple sclerosis.[28] However, the drug side effects (rash, dizziness, and dental discoloration) were frequent in the patients treated with minocycline, and in cases resulted withdrawal from the trial.[28] These further indicate the necessity of using brain-targeted delivery systems such as nanoparticles or nanocarriers to minimise drug side effects. Administration of selective MMP-9 inhibitor (SB 3CT) improved long-term neuro-behavioural in a mouse model of traumatic brain injury following intraperitoneal administration.[29] SB 3CT and its metabolite ρ-OH SB 3CT were rapidly adsorbed and distributed to the brain,[29] however, SB 3CT exhibits poor water solubility, which might have prevented its use in clinical trials since its discovery in 2000.[30] Therefore, clearly there is a need for brain targeting MMP-9 inhibitor with minimal side effects, low cost and scalability.

The present study was inspired by the work of Koivunen, E. *et al* 1999, who found that the synthetic peptide CTTHWGFTLC (cyclic disulfide-bonded) is a potent inhibitor of MMP-9,[31] although other MMP-9 inhibiting peptides have been reported.[32-34] Furthermore, CTTHWGFTLC is a water-soluble peptide[31], and it is relatively a short peptide, which would be an advantage in a large-scale production. This study aimed to synthesis amphiphilic peptides that self-assemble to form NPs incorporating the MMP-9 inhibiting peptide with the ability to cross the BBB for the treatment of neurodegenerative diseases and brain injuries. This work developed NPs containing a brain targeting peptide sequence (HAIYPRH) [HAI peptide], but not for a specific brain disease (Figure 1). *In vitro* experiments were conducted to evaluate the efficacy of the NPs in inhibiting MMP-9 enzyme and cytotoxicity of these NPs. In this work

we employed the hCMEC/D3 cell line to develop static *in vitro* BBB model.[35,36] Amphiphilic peptides have been developed previously to target the brain, [37,38] but not for the treatment of brain diseases such as stroke or MS. This study was a proof-of-concept that brain targeting NPs containing MMP-9 inhibiting peptide are able to reduce MMP-9 activity and cross the BBB.

2. Materials and Methods

2.1 Materials

All L-Fmoc amino acids, Oxyma and ProTide® resin were from CEM (Buckingham, UK). N,N′-Diisopropylcarbodiimide (DIC), piperidine, cholesteryl chloroformate (CHF), trifluoroacetic acid (TFA), triisopropylsilane (TIPS), acetonitrile, formic acid and N,N-diisopropylethylamine (DIPEA), trizma base (Tris), sodium chloride, Brij35, N-(3-Aminopropyl) methacrylamide hydrochloride (APMA) and cellulose dialysis tubing with molecular weight cut-off 10000 were from Sigma-Aldrich (Dorset, UK). Fmoc-L-4-fluorophenylalanine was from Fluorochem® (Hadfield, UK). Dimethylformamide (DMF), 1-(2-Pyridylazo)-2-naphthol (PAN) and diethyl ether were from Acros Organics® (Loughborough, UK). MMP-9 recombinant human protein, His Tag (10327H08H5), Pierce LDH cytotoxicity assay kit and calcium chloride dihydrate ($CaCl_2$) were from ThermoFisher Scientific® (Paisley, UK). hCMEC/D3 cell line and EndoGRO-MV kit media supplemented with (EndoGRO-LS supplement, rh EGF, L-Glutamine, Hydrocortisone hemisuccinate, heparin sulfate, ascorbic acid and fetal bovine serum) were purchased from Merck Millipore (Massachusetts, USA). Passage number used was from 1-11 with Lot number of 3130216. Carbon coated Cu grids were from Agar Scientific Ltd (Stansted, UK). FITC-dextran with a molecular weight of 70 kDa was purchased from Sigma-Aldrich (Dorset, UK). Polyethylene terephthalate 0.4 μm inserts (Sarstedt, Leicester, UK) were obtained from Sarstedt.

2.2. Methods

2.2.1. Solid-Phase Peptide Synthesis (SPPS)

Peptides were synthesised using a CEM Liberty Blue® automated microwave-assisted peptide synthesiser.[39] Briefly, 147 mg of Rink Amide ProTide resin (loading capacity 0.61 mmol/g) was transferred into a reaction vessel and was swollen in DMF. Typical Fmoc-deprotection required 20% piperidine in DMF for 90 seconds at 90ºC. 1 M DIC and Oxyma solutions were used as activator and coupling reagents, respectively. 0.2 M solutions of amino acids in DMF were used for synthesis. Amino acids were single coupled at 90ºC, except cysteine (Cys) coupled at 50ºC and arginine (Arg) double coupled at 75ºC.

2.2.2. Liquid Chromatography-Mass Spectrometry (LC/MS) Analysis

The validity of the synthesis was confirmed by high performance liquid chromatography (HPLC) and liquid chromatography and mass spectroscopy (LC/MS), as reported previously.[39] When the synthesis of peptides was accomplished, peptides were dispersed in 1 mL of MeOH and 0.1 mL of water respectively and sonicated for 15 minutes until fully dispersed prior to characterisation by liquid chromatography-mass spectrometry (Waters 2695 Separation Module linked with Quattro Premier Micromass). Samples were prepared in a mixture of water, acetonitrile and formic acid (80%: 20%: 0.1%) and separated (20 µL injection) on a XBridge® Peptide BEH C18 column (130 Ă, 5 µm and 4.6 mm x 150 mm) using a gradient elution of two mobile phases (A - water: formic acid 99.9%: 0.1%, B - methanol: formic acid; 99.9%: 0.1%). LC/MS (ESI in positive/negative switching mode, mass range 0-2000 Da) was used confirm the required *m/z* of the peptides present as well as other molecules/ impurities present. The tandem mass spectrum was used against the database to search for the required *m/z*. Analysis was performed using MassLynx mass spectroscopy software (Waters).

2.2.3. High Performance Liquid Chromatography (HPLC)

Synthesised peptides were characterised using analytical HPLC as reported previously.[39] Agilent 1200 Series was employed for HPLC analysis. A small amount of the sample was dissolved in 1 mL of MeOH and 0.5 mL of deionized water. The injection volume was 20 µL and the UV detection was 224-280 nm. Phenomenex C18 analytical HPLC column (3.6 µm particle size, 4.6 × 150 mm column) with a binary eluent system comprising MeOH / H_2O (18 min gradient: 5-95% with 0.1% formic acid) as mobile phase. Operating pressures were in the range of 2000-3000 PSI.

2.2.4. Conjugation of CHF to Peptides

Once the peptide sequence was synthesised and chemical structure was analysed, conjugation of CHF was commenced to produce amphiphilic peptides, as reported previously.[37] Briefly, ProTide resin-bound peptide (1 eq. based on loading capacity 0.61 mmol/g) was added to a solution containing CHF (2 eq.) and DIPEA (4 eq.) in DMF (4 mL) at 40^{o}C.[37] The Kaiser test was performed to assess the completeness of conjugation and the process was repeated until complete coupling. The amphiphilic peptide was cleaved from the resin by reacting with 5 mL of cleavage cocktail [comprising TFA, TIPS and water (9:0.5:0.5 *v/v*)] with regular shaking at room temperature for 4 h. The solution was then filtered into ice cold diethyl ether followed by centrifugation. Precipitated amphiphilic peptide was repeatedly resuspended in diethyl ether with subsequent centrifugation for three times. Diethyl ether was evaporated by leaving it overnight in the fridge. Amphiphilic Peptides were dispersed in water, flash frozen and freeze dried to obtain the conjugated peptide as powder. No further steps were taken to cyclise the cysteine amino acids in the peptides or purify the conjugated peptides. Excess TFA was removed by lyophilisation after cleavage/precipitation of the conjugated peptide. Therefore, the conjugated peptide was a TFA salt.

2.2.5. MMP-9 Enzyme Activation

The enzyme activation was achieved by following manufacturer's protocol. A TCNB buffer [Tris (50mM), $CaCl_2$ (10mM), NaCl (150 mM) and Brij 35 (0.05%)] was prepared using Trizma base (Tris) at a concentration of 200 mM, calcium chloride dihydrate ($CaCl_2$) at a concentration of 40 mM, sodium chloride (NaCl) at a concentration of 600 mM, Brij35 at a concentration of 0.2%. Each of these components was dissolved in 10 mL of sterile water separately, then 1 mL from each solution was transferred into another container and the desired concentration was achieved. To the 5 μg MMP-9 (ThermoFisher, REF – 10327-H08H-5, LOT –LCL09AU0402) 900 μL of the TCNB buffer was added in 100 μL increments to dissolve the sample. Then, 100 μL of APMA was added to give a concentration of 1 mM. The final solution of MMP-9 was obtained with the concentration of 64.4 nM. This solution was incubated for 24 h at 37°C. Following this, 3 mL of TCNB buffer was added to make a 16 nM solution of MMP-9. One mL of this solutions was further diluted to 8 mL in TCNB buffer to give a 2 nM solution for use in NMR studies.

2.2.6. Dynamic Light Scattering (DLS) analysis and Zeta Potential Measurement

Particle size was measured by using Malvern Zetasizer Nano ZS® (Malvern, Worcestershire, UK), containing a He-Ne laser source (λ= 632.8 nm, 22 mW output power). Cuvettes used were DTS0012. The refractive index of 1.3 and viscosity of 0.9 cP were used for water. Three readings were performed on the amphiphilic peptide samples dispersed in water. The same instrument was used to measure the zeta potential. All measurements were carried out in triplicates, means and standard deviations (SD) were also calculated.

2.2.7. Transmission Electron Microscopy (TEM)

Peptide nanocarriers were visualised and characterized morphologically by FEI Morgagni transmission electron microscope. Carbon filmed copper grids were used. 2.5 mg/mL peptide solution was prepared in distilled water. A small droplet of the peptide solution was placed on

the grid and left to dry. Samples were analysed in the TEM after drying. No staining (negative of positive) was used.

2.2.8. Preparing Nanoparticle Dispersions

Sterile deionised water was used to prepare nanoparticle dispersions. The procedure was carried-out in a disinfected laminar flow cabinet to prepare 2.5 mg/mL suspension of the amphiphilic peptide. Bath sonication of the suspension was then carried out for 1 h and 45 min to disperse the amphiphilic peptide particles and form the nanoparticle colloidal dispersions VWR Ultrasonic Cleaner USC 300 TH 2.8 L 45 kHz (VWR International) with 160 W (effective 80 W) ultrasonic power.

2.2.9. Dialysis

Approximately 15 cm of dialysis tubing was soaked in a beaker of water for 5 min. In a separate beaker, 40 mL of distilled particle free water was added with a magnetic stirrer bar. Once the tubing was flexible, one end was tied, 1 ml of the amphiphilic peptide nanocarrier suspension was placed inside it and the other end was tied to seal. This was then placed into the 40 mL of water (40-folds dilution) containing the magnetic bar; secured using an elastic band and then the beaker was placed on a stirring plate. The parameters on the fluorescence spectrophotometer were set with excitation at 270 nm, emission starting at 300 nm and stopping at 400 nm with the slit width set at 20 nm. The background fluorescence was measured using just water in a four clear side quartz cuvette using the fluorescence spectrophotometer (VARIAN CARY Eclipse, UK). The intensity of fluorescence of the surrounding water was then tested at time 0, 1, 2, 3, 4, 5, 6 and 24 h. At each sampling time point, 3 mL (1x 3 mL) from outside of the dialysis bag was placed in the 4-clear side cuvette and analysed using the fluorescence spectrophotometry and the intensity was measured to determine the release of the amphiphilic peptide through the dialysis membrane. Each sample was returned to the beaker after each test to keep the volume at 40 mL.

The same dialysis procedure was then carried out with the NPs dispersed in fetal bovine serum (FBS) with distilled water on the outside of the bag. All release studies replicated three times.

2.2.10. Enzyme Inhibition Study and Enzyme Kinetic Evaluations

Enzymatic studies (inhibitory effects of NPs) were conducted by using the Bruker® Ascend™ 600 MHz NMR spectrometer. One-dimensional (1D) fluorine-19 (^{19}F; 564.7 MHz) NMR experiments were performed with proton decoupling at room temperature (298 K). An in-house developed highly sensitive MMP-9 peptide (TY-26, results due to be published separately) with 4-fluorophenylalanine was used to analyse the inhibitory effects of NPs. A sample (350 µL) of MMP-9 sensitive peptide (5 mg/mL) was added to NMR tube along with 400 µL of the activated MMP-9. This was the control sample. The same solution and 350 µL of MMP-9 inhibiting nanocarrier aqueous dispersion was added to the second NMR tube as the test sample. Peptide products and metabolites containing 4-fluorophenylalanine were observed as singlets with different characteristic chemical shifts. Chemical shift values were calibrated to TFA (-76.55 ppm) as the internal standard. Data obtained was viewed and analysed by using TopSpin® and Dynamics centre 2.4.5 (Bruker®) was used for processing and calculating enzyme kinetics. Further control tests were conducted by evaluating MMP-9 sensitive peptide in the TCNB buffer and degradation of an MMP-9 non-responsive peptide (TY-27: GGYGQ-GYW^{19}FG) in the presence of MMP-9.

2.2.11. Assessment of Cell Death Induction

The lactate dehydrogenase (LDH) assay was used to assess the potential toxicity of the MMP-9 inhibitory NPs. HeLa cells were grown in Dulbecco's Modified Eagle Medium (DMEM) supplemented with 10% FBS and 2 mM L-glutamine. They were then washed with phosphate-buffered saline, trypsinised, re-suspended in the growth medium, counted and seeded into an opaque, micro-clear, flat bottom 96 well tissue culture plate at a density of 7.5

x 10^4 cells/mL (7500cells/ well at 100 µL/well). A blank control well with no cells (complete medium only) was included. The experimental design included triplicate wells to be later used for LDH assay controls. The 96 well plate was then incubated overnight at 37°C with a 5% CO_2 supply. Then the nanocarriers were added to the culture wells in triplicate. Sterile water was added to the negative control wells. The treated 96 well plate was then incubated for 24 h at 37°C and 5% CO_2, at the end of which, the LDH assay was carried out according to the manufacturer's protocol (ThermoFisher, Pierce LH Cytotoxicity Assay Kit, Cat. No. 88953). Included in the design were a spontaneous LDH activity control (10 µL of sterile water, to capture minimum LDH release, i.e., completely healthy cells representing 0% LDH release) and a maximum LDH activity control (10 µL of 10x lysis buffer, expected to fully lyse the cells, indicative of 100% LDH release). The 96 well plate was then incubated for a further 45 min at 37°C with a 5% CO_2 supply. Following this incubation, 50 µL of medium from each test or control well was transferred into a new 96 well flat-bottom plate. Then 50 µL of reaction mixture was added to each of these wells and the plate was tapped gently. This plate was then incubated at room temperature for 30 minutes whilst covered in foil to protect it from light, after which, 50 µL of stop solution (strong acid) was added to each of the wells and was mixed by gentle tapping. Any bubbles made were removed with a syringe needle. Then with the Clariostar plate reader (BMG Labtech), the value for the blank well (non-cell-containing) was subtracted from the negative control value and each treatment value. The resultant value at 680 nm was then subtracted from the corresponding resultant value at 480 nm. These final values were then analysed by expressing the value for the negative control or for each treatment as a percentage of the maximum LDH release value. Three cell passages were studied.

2.2.12. Blood Brain Barrier In Vitro Model Preparation and Transmigration Assay

The BBB *in vitro* model was constructed using protocol supplied by Merck Millipore. Permeability across the BBB was conducted by using an *in vitro* BBB model utilising

immortalized human brain endothelial cell line hCMEC/D3. Briefly, 90000 cells were seeded in 24 well TC-inserts and 500 µL of EndoGRO culture media with supplements (including serum and VEGF) was added; and 1.6 mL of the same medium was added in the well containing the insert. The plate was placed in the incubator at 37ºC with 5% CO_2. After 24 h, transepithelial/endothelial electrical resistance (TEER) was measured by using EVOM^2 (world precision instruments, USA). Prior to the permeability experiment, sensitivity of the BBB monolayer was tested by using histamine and cimetidine. Briefly, media were replaced and histamine was added in to inserts at a final concentration of 50 µM. The plate was incubated for 30 min at 37ºC. TEER values were measured at 36 h. Cells were washed with sterile PBS buffer and fresh media were added. Cimetidine was added into inserts at a final concertation of 50 µM. The plate was incubated for 1 h and TEER values were measured. Culture media were replaced with fresh media and incubated for 12 h. TEER values were measured again after 48 h. Furthermore, TEER values were determined after transmigration tests. All measurements were carried out in triplicates, means and standard deviations (SD) were also calculated.

For transmigration studies, hCMEC/D3 cells were seeded at 90000 cells/insert for 48 h and TEER values were measured to ensure formation of the biological barrier. The media were replaced with fresh media and NPs were added to the apical side to achieve final concentration of 0.4 mg/mL. Concentration of NPs transmigrated the BBB monolayer was assessed by measuring the fluorescence in basolateral compartment at λ_{exc} 270 nm and λ_{ems} 341 nm by using SpectraMax i3x Multi-Mode Detection plate reader (Molecular Devices, USA).

The transmigration of NPs across the BBB was calculated from Equation 1:

$$\%\ of\ NPs\ in\ Basal\ Chamer = \frac{Fluorescence\ of\ NP\ at\ time\ t\ in\ basal\ chamber}{Flurorescence\ of\ Total\ NP\ in\ basal\ chamber} \times 100$$

Equation 1

Where “Fluorescence of Test NP at time t in basal chamber” indicates the fluorescence of NPs in the basolateral compartment at a certain time t; and “Fluorescence of Total NP” denotes the fluorescence of NPs when all NP sample was added into the basolateral compartment. Apparent permeability (Papp) was calculated as reported previously.[40]

After final fluorescence measurements of NPs at time 24 h in the basolateral compartment, TEER values were measured again and media replaced with pre-heated fresh media. 10µL of FITC-Dextran solution (1mg/mL) was added to the apical side and florescence (λ_{exc} 485 nm, λ_{ems} 520 nm) was measured in the basolateral compartment. The experiments were replicated in three separate runs.

2.2.13. Statistical Analysis

GraphPad Prism Software 8.0.1 for Windows (GraphPad Software, Inc., La Jolla, CA, USA) was used to conduct one-way analysis of variance (ANOVA) followed by Tukey’s post-hoc test for multiple comparisons in order to identify any statistically-significant differences between the means of treatment groups. For statistical comparisons, $P<0.05$ was considered a statistically significant difference.

3. Results

3.1. Characterisation of Chemical Structure, Size Distribution, and Morphology of Nanoparticles

Three types of amphiphilic peptides were examined (Table 1). In these compounds two types of brain targeting ligands were examined: MiniAp-3 (CKAPETALC),[41] and HAI peptide (HAIYPRH).[42] In addition, at the N terminus of the MMP-9 inhibitor peptide three glycine residues were incorporated as a spacer between the MMP-9 inhibitor peptide and cholesterol. The HPLC data (supplementary information S1 and S2) suggested the formation of disulphide bridges between cysteine amino acids in Peptide **1** and also Peptide **2** (peaks at retention time

of 13.7 and 14.0 min in Figure S1 and peaks at 15.9 and 16.4 min in Figure S2). For Peptide **3** the peak at 17.5 min (Supp. Figure S3) would suggest the formation disulphide bridges between the cysteine amino acids in the peptide. These observations suggest *in situ* cyclisation of peptides (but not complete) upon cleavage of peptides from the resin, despite no intentional steps being taken to cyclise the peptides. LC/MS data confirmed successful synthesis of Peptide **3** (Figure S4). Among these peptides, only peptide **3** with the sequence GGGCTTHWGFTLCHAIYPRH was successfully conjugated with cholesterol. The other two peptides did not show the conjugation with CHF by performing the Kaiser test. Therefore, the following results are presented for Peptide **3**. LC/MS data and UV chromatogram indicated the conjugation of CHF to the peptide sequence (Supp. Figure S5 and S6). The calculated mass for conjugated Peptide **3** was 2626.13 Da; and m/z at 1314.5 was indicative of the doubly charged conjugated Peptide **3** with m/z at 876.9 indicating triply charged peptide and m/z at 738.5 showing fragmentation of Peptide **3** from CHF. The MMP-9-inhibitor NPs had average size of 202.8 ± 105.6 nm, with polydispersity index (PdI) of 0.2 (Figure 2), and zeta potential of +26.7 mV. TEM images revealed irregular shape for MMP-9 inhibitor NPs (Figure 3). As this was a preliminary study and our expectation was that only conjugated peptides would form nanoparticles, then, we did not purify the conjugated peptide.

3.2.MMP-9 Inhibition Studies

Figure 4A presents typical change in the NMR signal for the MMP-9 cleavable peptide (TY-26) in the presence of MMP-9 enzyme over 20 h. It can be seen that the intact peptide signal (-117.5 ppm) gradually decreases and a degradation product signal (-117.2 ppm) appears. The degradation product signal becomes clearly visible after 20 h. The degradation rate constant for the MMP-9 cleavable peptide was $4.5\times10^{-6}s^{-1}$. On the other hand, the cleavage of TY-26 was completely blocked by the MMP-9 enzyme in the presence of MMP-9 inhibitor NPs (Figure 4B). In the duplicate run, it was found that the cleavage of TY-26 decreased to

$1.9\times10^{-6}s^{-1}$ in the presence of MMP-9 enzyme and MMP-9 inhibitor NPs (Supplementary Figure S7). The variations in the cleavage of TY-26 could be due to the impurities in the NPs. The TY-26 did not degrade noticeably in the presence of the TNCB buffer (Figure S8). Also, MMP-9 non-responsive peptide (TY-27) did not degrade in the presence of MMP-9 (Figure S9). These control tests suggest inhibition of TY-26 degradation in the presence of MMP-9 enzyme and MMP-9 inhibiting NPs.

3.3.Non-Toxicity of MMP-9 Inhibiting Nanoparticles

Figure 5 shows the outcomes of the experiment assessing the potential effects of the MMP-9 inhibiting NPs on LDH release. An increase in LDH release indicates increased cell death. The NPs at the tested concentrations did not induce any LDH release that was significantly different to that of negative. The percentage LDH release for the negative control was 18.2 ± 2.6%, while for the NPs at 0.06 mg/mL, 0.14 mg/mL and 0.25 mg/mL it was 19.3 ± 3.3%, 19.3 ± 4.7% and 17.1 ± 2.6%, respectively. One-way-ANOVA did not show a statistical difference between the control cells and treated cells (all concentrations) in percentage of LDH release (P=0.9*).*

3.4.In Vitro Disintegration of MMP-9 Inhibiting Nanoparticles Using Dialysis

The disintegration (release) studies were conducted to determine whether the MMP-9 inhibiting NPs would dissemble upon dilution, for example after intravenous injection. Figure 6 presents that fluorescence intensity increased slightly from 155.7 ± 28.7 a.u. to 235.2 ± 33.9 a.u. in the release media after 6 h incubation of the NPs in 40 mL of distilled water. A typical fluorescence curve is presented in Figure S10. This indicates that MMP-9 inhibiting NPs would have critical micelle (aggregation) concentration much less than 37 mg/L. However, the fluorescence intensity increased significantly from 158.7 ± 30.8 a.u. to 445.1 ± 68.1 a.u. in the release media for the MMP-9 inhibiting NPs in 24 h, when these were incubated with FBS. However, the degradation appeared in a two-step process. It can be seen from Figure 6 that in

the step-one the fluorescence intensity increased only from 158.7 ± 30.8 a.u. to 218.9 ± 27.9 a.u. in 5 h incubation in the presence of FBS. Then, the fluorescence intensity jumped to 445.1 ± 68.1 a.u. in 24 h incubation in the presence of FBS. This observation suggested the degradation of the NPs by the enzymes in the serum, and not disintegration of the NPs up on dilution. Furthermore, the MMP-9 inhibiting NPs would not degrade rapidly by the serum enzymes.

3.5.The In Vitro BBB Transmigration of MMP-9 Inhibiting Nanoparticles

The TEER values of BBB model reached 239 ± 28 Ω cm^2 after 48 h of incubation; and slightly increased to 250± 13 Ω cm^2 after the treatment of the cells with MMP-9 inhibiting NPs. Histamine treatment resulted in the reduction of TEER values from 200Ω cm^2 to 62 Ω cm^2. Whereas treatment with cimetidine helped the TJ to restore their integrity up to 145Ω cm^2 as shown in Figure 7.

The MMP-9 inhibiting NPs showed an ability to cross the *in vitro* BBB (Figure 8). The percentage of NPs that crossed the BBB model reached 23 ± 5% after two hours of incubation and reached 28 ± 3% at 5 h. However, Figure 8 shows a decrease, although not significantly, in the number of NPs that transmigrated from the apical side of the BBB model to the basolateral side after 5 h and reduced to 22% ± 3% at 24 h. This trend was more pronounced when Papp was calculated (Figure 9). It can be seen from Figure 9 that Papp decreased after 2 h post incubation, indicating that there was not net increase in the transmigration of NPs in the basolateral compartment. The negative values of Papp highlights net decrease in the total number of NPs in the basolateral compartment. This observation suggests return of some NPs from the basolateral side of the model to the apical side. After treatment of cell with the NPs, it was observed that only 0.5 ± 0.1% of FITC-dextran crossed the *in vitro* BBB model, indicating NPs did not compromise the BBB permeability.

4. Discussion

This work demonstrated the preparation of hard-core peptide-based NPs containing brain targeting ligand, with MMP-9 inhibition properties. The NPs were shown to be non-toxic with an average diameter of 200 nm. The NPs were able to reduce the activity of the MMP-9 enzyme either completely or by half in a ^{19}F NMR based assay. Importantly, the NPs maintained their integrity upon dilution, but could be hydrolysed gradually by the enzymes in the serum. Furthermore, the MMP-9 inhibiting NPs showed the ability to cross an *in vitro* BBB model. In this work, we did not investigate the ability of NPs without brain targeting ligands. This was based on observations made by other investigators that inclusion of brain targeting ligands improves significantly the ability of NPs to cross the BBB following intravenous administration.[43-47]

In a previous study, magnetic NPs-bound TMP-1 had the size of 10 ± 3 nm,[17] and similarly surface adsorbed siRNA on quantum dots (QD–siRNA nanoplexes) had a diameter of 15-20 nm.[16] These are much smaller than the MMP-9 inhibiting NPs we present in this work, however, our NPs exhibited an irregular shape compared to previous work.[16,17] The PdIs were similar for the magnetic NPs,[17] and MMP-9 inhibiting NPs of this work. In another study, the diameters of PLGA NPs encapsulating TMP-1 were between 80 nm and 430 nm (depending on TMP-1 loading);[18] and the PLGA NPs had spherical shape. Furthermore, Cu@mSiO_2-PEG NPs showed MMP-9 inhibiting properties in HeLa cells.[48] These NPs also had an irregular shape, but with an average diameter of 179.7 nm.[49] Therefore, the MMP-9 inhibiting NPs of our work had sizes within the range of previous works. Moreover, the relatively large size of these NPs would be expected to make them reside at the basal lamina of the BBB.[50] This would be beneficial, as MMP-9 at the BBB increases the permeability of the BBB, which results in neuronal damage.[51]

Researchers have developed formulations to reduce the expression of MMP-9. For example, Cu@mSiO$_2$-PEG NPs reduced the expression of MMP-9 in HeLa cells, [48] and QD–siRNA nanoplexes reduced the expression of MMP-9 in brain microvascular endothelial cells by 78%. In addition, solid lipid NPs-encapsulating MMP-9 downregulating shRNA-reduced the secretion of MMP-9 in human corneal epithelial cells by 30%.[52] The ability of our NPs to inhibit MMP-9 was investigated through the use of a specially-designed and optimised ^{19}F NMR based assay that measures the remaining ^{19}F-labelled peptide upon treatment with MMP-9 compared with control. MMP-9 inhibiting NPs of this study had concentration of 480 µM and they reduced the activity of MMP-9 completely or by half. The variation in the MMP-9 inhibiting properties of the NPs could be due to the impurities in the NPs. Therefore, further experiments are required using purified conjugated peptides to verify this hypothesis. The CTTHWGFTLC peptide inhibited MMP-9 with an IC_{50} of about 500 µM.[31] Therefore, the MMP-9 inhibiting NPs containing CTTHWGFTLC peptide showed comparable inhibiting activity to the parent peptide alone in solution. In another study, gold NPs stabilised by polyvinylpyrrolidon (PVP) blocked completely MMP-9 activity at 400 µg/mL.[53] The gold nanoparticle concentration was significantly lower than the MMP-9 inhibiting nanoparticle concentration (1.25 mg/mL) in our MMP-9 inhibiting study. Hence, the gold NPs are more efficient in inhibiting MMP-9 compared to peptide-based MMP-9 inhibiting NPs. However, it should be noted that gold NPs may activate microglia,[54] while the MMP-9-inhibiting NPs can be digested by enzymes in the body.

The MMP-9 inhibiting NPs in this work, up to 250 µg/mL, did not present significant toxicity towards HeLa cells, and other nanoparticle formulations also showed similar findings;[17,52,53] while PVP-coated platinum NPs did show cell toxicity at 100 µg/mL concentration.[53] Furthermore, magnetic NPs-bound TMP-1 NPs showed cell toxicity at concentrations above 10 µg/mL.[17] These observations indicate that the MMP-9 inhibiting NPs

in our work, even at concentrations as high as (250 µg/mL), do not present any toxicity issues. Unlike certain previously reported formulations.[17,53] In this work, we evaluated the toxicity of MMP-9 inhibiting NPs in HeLa cells (as divide and grow unusually fast), similar to a previous work.[55] This was mainly due to the presence of serum in the culture media of hCMEC/D3, which potentially digest the MMP-9 inhibiting peptides, and mask the toxic effects of the NPs. However, the TEERs values of the BBB model did not decrease following treatment with the MMP-9 inhibiting NPs. This could also show nontoxic effects of the NPs towards hCMEC/D3 cells, as it has been shown that cytotoxic materials decreases TEER values of *in vitro* BBB models.[56] Perhaps, the toxicity studies may also be conducted in brain endothelial cells and neuronal cells.[16,17]

Amongst the nanoparticle formulations discussed above, the PVP stabilised gold NPs,[53] CuS@mSiO2-PEG NPs,[48] and MMP-9 inhibiting NPs of our work did not require loading of an active ingredient, such as TIMP-1.[16-18,52] Therefore, the MMP-9 inhibiting NPs of our study would have fewer challenges in scale-up compared to the other approaches for the treatment of brain diseases, when undesired activity of MMP-9 increases in the brain. However, it should be noted that, we noticed a slow conjugation process for the cholesteryl chloroformate. Hence, further research will be required to optimise this process, or even to replace the cholesteryl motif with a more synthetically-tractable hydrophobic peptide sequences that will lead to the formation of NPs by self-assembly of these amphiphilic peptides in aqueous media;[57-63] leading to improved scale-up. In this approach, it would be required to conduct studies using circular dichroism to determine the roles of peptide secondary structure in the formation of self-assembled nanoparticles.[64]

Here, we found that HAI peptide would conjugate more effectively to the MMP-inhibiting peptide (CTTHWGFTLC) compared to Mini-app3 (CKAPETALC). In a previous work polysorbate 80 was used to facilitate crossing the BBB by NPs.[18] While in another work, a 0.08

T magnetic field was employed to allow the magnetic NPs to cross an *in vitro* model of the BBB.[17] The use of brain targeting ligand makes no need to apply for a magnetic field. Also the use of polysorbate 80 may accumulate the NPs in the lungs.[19] However, only 28% (at the most) of MMP-9 inhibiting NPs of our work crossed the *in vitro* BBB, whilst this amount can reach around 40% for magnetic NPs under the influence of a magnetic field. It should be noted that the *in vitro* BBB model using hCMEC/D3 may not represent the physiological BBB barrier. As it has been shown that the barrier could be impermeable to FITC-dextran (MW 70 kDa) but permeable to smaller molecular weight of FITC-dextran (MW 4 kDa).[65] Furthermore, the BBB model used in our work lacked other components of the BBB such as astrocytes and pericytes, or being dynamic.[66-68] However, a good correlation has been observed between the *in vivo* and *in vitro* data by using a static monolayer of brain endothelia cells (like our model).[64,69] Ultimately, *in vivo* studies would further indicate the ability of the MMP-9 inhibiting NPs crossing the BBB. As *in vivo* studies will take into account crossing the BBB, binding to plasma proteins, clearance by the reticuloendothelial system, and enzymatic cleavage in the serum.[70] The MMP-9 inhibiting NPs of our work showed crossing of the *in vitro* BBB model 2 h after incubation. This is in agreement with previously published work.[17] It may be argued that during this period part of NPs might be cleared from the blood by the reticuloendothelial system. *In vivo* studies showed that significant brain uptake occured for exosome coated gold nanoparticles, when after 3 h only 10% of the exosomes crossed the *in vitro* BBB model.[69] This is to indicate that when *in vitro* data shows low levels of NPs crossing the BBB, the *in vivo* data may show complete the opposite.

Amphiphilic peptides containing cholesterol self-assembled to form nanoparticles and a critical micelle concentration (CMC) was measured.[37] Based on this observation, we speculate that NPs of our study formed by self-assembly. However, the long-duration of sonication to form irregular shape nanoparticles created a doubt that whether the amphiphilic peptides could

be dispersed at the molecular level in an aqueous media for CMC measurements. Although this property created an advantage that the NPs did not disintegrate upon dilution.

The availability of MMP-9 inhibiting NPs (like the ones in this study) can be useful for the treatment of ischemic stroke.[71] In a previous work, polymeric NPs were prepared by the copolymer of poly(ethylene glycol)-*b*-poly(D,L-lactide), and loaded with curcumin. The NPs had size distribution of 147.8 ± 5.7 nm. The nanocarriers were NOT decorated with brain targeting ligand, and they were injected intravenously to mice with ischemia/reperfusion injury. The nanocarriers appeared in the regions with ischemia/reperfusion injury, and reduced the expression of the MMP-9 in the ischemic cortex, which helped reducing the infarct size and improving function recovery.[72] The nanocarriers might have crossed the BBB through compromised tight junctions in the ischemic region.[72] It should be noted that the BBB is rapidly disrupted and the disruption remains for days in acute ischemic stroke.[73,74] The BBB permeability increased from 0.83 mL/100 g per minute to 1.15 mL/100 g per minute in the infarcted region of human brain.[73] Therefore, the BBB permeability increases for about 38%. This is still a strong barrier to allow sufficient NPs to cross the BBB. Therefore, as shown previously, more NPs penetrated to the brain, when the surface of NPs was decorated with brain targeting ligand, which presented with significantly improved therapeutic outcome.[75] These observations indicate that the surface of NPs should be decorated with brain targeting ligand to achieve significant/desired clinical outcomes for the treatment of ischemic stroke. Furthermore, patients with hyperglycaemia tend to have increased serum MMP-9 levels, and this makes them prone to stroke, due to compromised BBB.[76] Hence, a safe MMP-9 inhibiting NP formulation can be beneficial for these patients.

A previous study administered about an intraperitoneal dose of 0.5 mg/kg (12.43 μg per mouse) of a triple-helical MMP-9 inhibiting peptide to experimental autoimmune encephalomyelitis (EAE) mice; and the clinical severity of EAE reduced from day 12 (post

EAE induction) afterwards.[77] As these peptides did not contain brain-targeting ligand, but showed clinical efficacy, therefore it may be suggested that similar dose would be suitable for *in vivo* work. However, by considering that typically 1% of intravenously administered NP dose reaches the brain,[75] and 35 µL as CSF volume of mouse, then the MMP-9 inhibiting NP concentration in the brain will be 3.5 mg/mL with the dose of 12.42 µg per mouse. As our *in vitro* data showed reducing MMP-9 activity at 1.25 mg/mL, then for *in vivo* studies, the dose of 0.5 mg/kg may be sufficient to inhibit MMP-9 in the mouse brain. These calculations are based on the assumption that MMP-9 inhibiting NPs would cross the BBB *in vivo.*

There are limitations to this research. First, the MMP-9 inhibiting NPs should be tested *in vivo* where elevated MMP-9 levels in the brain cause neurodegeneration for example in EAE mice as reported previously.[77,78] This also would help to test the effects of protein corona on the efficacy of the NPs on inhibiting MMP-9. Second, peptides with different MMP-9 inhibitory activity should be included in the structure of NPs to test that whether MMP-9 inhibitory activity is derived solely from the MMP-9 inhibiting peptide. Third, the blood compatibility of the MMP-9 inhibiting NPs should be tested such as complement activation, haemolysis and platelet aggregation. In this work, we did not investigate the potential inhibition of other enzymes in the brain such as MMP-2 by our MMP-9 inhibiting NPs.[77] Therefore, this aspect should be taken into account, if exclusive inhibition of MMP-9 is needed.

5. Conclusion

Our work presents proof-of concept for the development of peptide based MMP-9 inhibiting NPs, which were able to reduce the activity of MMP-9 considerably. The NPs included the brain targeting HAI peptide ligand, which helped to cross an *in vitro* model of the BBB. Importantly, the NPs did not show cell toxicity up to 250 µg/mL concentration. Moreover, as compared to previous reported nanoparticle based formulations for brain drug delivery, these provide the advantages of scalability and of not needing to load the active

ingredient. Furthermore, the NPs had average diameter of 202.8 ± 105.6 nm with PdI of 0.2, which make them suitable to remain in the basal lamina of the BBB, where the activity of MMP-9 released from the endothelial cells or macrophages would compromise the BBB permeability. We envisage that the *in vitro* proof of concept described herein can serve as a platform for new *in vitro* and *in vivo* studies into the development a new class of brain-targeting MMP-9 inhibitors for the treatment of progressive neurodegenerative diseases and brain injuries, when undesired activity of MMP-9 increases.

6. Acknowledgment

We are grateful for technical assistance of Olivia Franklin, Osekafore Alabi and Chloe Geraghty.

7. Confilict of Interest

The authors declare no conflict of interest.

8. List of Figures and Tables

Table 1: Peptide sequences that were synthesised and theoretical molecular mass, where C was TRT protected.

Figure 1: A) Schematic diagram of the formation of self-assembled MMP-9 inhibiting NPs by amphiphilic peptides. B) Ball and stick presentation of the MMP-9 inhibiting amphiphilic compound: Cholesterol-CTTHWGFTLCHAIYPRH. Cholesterol is presented as yellow ball and sticks.

Figure 2: Particle size distribution report of MMP-9 inhibiting nanoparticles obtained by the DLS method. This figure shows three different measurements. The average particle size and PdI are presented at the top of figure.

Figure 3: TEM images of MMP-9 inhibiting NPs, presenting irregular shape of NPs. The scale bar is 500 nm.

Figure 4: ^{19}F NMR data presenting the inhibition of MMP-9 by MMP-9 inhibiting NPs. A) Cleavage of a MMP-9 cleavable peptide (TY-26) by MMP-9 enzyme is represented by disappearing signal at -117.5 ppm and appearance of enzyme degradation product signal at -117.2 ppm, B) The inhibition of TY-26 cleavage by MMP-9 inhibiting NPs in the presence of MMP-9 enzyme is shown by persistent signal at -117.6 ppm and no any other signals.

Figure 5: Cell toxicity of MMP-9 inhibiting NPs towards HeLa cells measured by LDH release. Lack of toxicity of MMP-9 inhibiting NPs is indicated by LDH release comparable to control tests. LDH release is expressed as mean ± SD (n=3).

Figure 6: Release of MMP-9 inhibiting NPs (MIB-NPs) from a dialysis bag with or without the presence of foetal bovine serum (FBS), presenting degradation of MIB-NPs by enzymes in the FBS and slight disintegrations of MIB-NPs upon dilution. Error bars present SD (n=3).

Figure 7: TEER values for *in vitro* BBB prepared by hCMEC/D3 cells seeded at 90000/insert after 24 h, 36 h, post histamine and post cimetidine treatment, presenting formation of a biological barrier that can be compromised by pharmacological compounds (histamine) and restated by pharmacological agents (cimetidine). Error bar indicate SD (n=3).

Figure 8: Transmigration study of MMP-9 inhibiting NPs using hCMEC/D3 *in vitro* BBB model, demonstrating ability of the NPs to cross the BBB after 2 h incubation at 37°C. Also, the figure presents gradual drop in transmigrated NPs to the basolateral compartment after 5 h incubation. Error bars present SD (n=3).

Figure 9: The relationship between *in vitro* brain permeability and time for MMP-9 inhibiting NPs using hCMEC/D3 cell line. It can be seen that Papp reduced considerably after 2 hr incubation and it was negative after 5 hr incubation. This observation suggests reverse of NPs from the basolateral compartment to the apical compartment. Error bars present SD (n=3).

9. References

1. Tallant C, Marrero A, Gomis-Rüth FX 2010. Matrix metalloproteinases: Fold and function of their catalytic domains. Biochimica et Biophysica Acta (BBA) - Molecular Cell Research 1803(1):20-28.
2. Li X, Zhao Y, Chen C, Yang L, Lee H-h, Wang Z, Zhang N, Kolonin MG, An Z, Ge X, Scherer PE, Sun K 2020. Critical Role of Matrix Metalloproteinase 14 in Adipose Tissue Remodeling during Obesity. Molecular and Cellular Biology 40(8):e00564-00519.
3. Itoh Y 2006. MT1-MMP: A key regulator of cell migration in tissue. IUBMB life 58(10):589-596.
4. Pittayapruek P, Meephansan J, Prapapan O, Komine M, Ohtsuki M 2016. Role of Matrix Metalloproteinases in Photoaging and Photocarcinogenesis. International journal of molecular sciences 17(6):868.
5. Reinhard SM, Razak K, Ethell IM 2015. A delicate balance: role of MMP-9 in brain development and pathophysiology of neurodevelopmental disorders. Front Cell Neurosci 9:280-280.
6. Nagase H, Visse R, Murphy G 2006. Structure and function of matrix metalloproteinases and TIMPs. Cardiovascular research 69(3):562-573.
7. Liotta LA, Tryggvason K, Garbisa S, Robey PG, Abe S 1981. Partial purification and characterization of a neutral protease which cleaves type IV collagen. Biochemistry 20(1):100-104.
8. Hadass O, Tomlinson BN, Gooyit M, Chen S, Purdy JJ, Walker JM, Zhang C, Giritharan AB, Purnell W, Robinson CR, II, Shin D, Schroeder VA, Suckow MA, Simonyi A, Y. Sun G, Mobashery S, Cui J, Chang M, Gu Z 2013. Selective Inhibition of Matrix Metalloproteinase-9 Attenuates Secondary Damage Resulting from Severe Traumatic Brain Injury. PloS one 8(10):e76904.
9. Brkic M, Balusu S, Libert C, Vandenbroucke RE 2015. Friends or Foes: Matrix Metalloproteinases and Their Multifaceted Roles in Neurodegenerative Diseases. Mediators of inflammation 2015:620581.
10. Kumari R, Willing LB, Patel SD, Baskerville KA, Simpson IA 2011. Increased cerebral matrix metalloprotease-9 activity is associated with compromised recovery in the diabetic db/db mouse following a stroke. J Neurochem 119(5):1029-1040.
11. Inzitari D, Giusti B, Nencini P, Gori AM, Nesi M, Palumbo V, Piccardi B, Armillis A, Pracucci G, Bono G, Bovi P, Consoli D, Guidotti M, Nucera A, Massaro F, Micieli G, Orlandi G, Perini F, Tassi R, Tola MR, Sessa M, Toni D, Abbate R 2013. MMP9 variation after thrombolysis is associated with hemorrhagic transformation of lesion and death. Stroke 44(10):2901-2903.
12. Nyormoi O, Mills L, Bar-Eli M 2003. An MMP-2/MMP-9 inhibitor, 5a, enhances apoptosis induced by ligands of the TNF receptor superfamily in cancer cells. Cell Death & Differentiation 10(5):558-569.
13. Nguyen TT, Ding D, Wolter WR, Pérez RL, Champion MM, Mahasenan KV, Hesek D, Lee M, Schroeder VA, Jones JI, Lastochkin E, Rose MK, Peterson CE, Suckow MA, Mobashery S, Chang M 2018. Validation of Matrix Metalloproteinase-9 (MMP-9) as a Novel Target for Treatment of Diabetic Foot Ulcers in Humans and Discovery of a Potent and Selective Small-Molecule MMP-9 Inhibitor That Accelerates Healing. Journal of Medicinal Chemistry 61(19):8825-8837.
14. Zavodovskaya M, Zhang Y, Xiao Y, Maltzman J, Smith V, Brachmann CB, Patterson SD 2017. Abstract 4663: Exploratory serum biomarker analysis in gastric cancer patients

treated with GS-5745, an MMP9 Inhibitor, in combination with mFOLFOX6. Cancer Research 77(13 Supplement):4663-4663.
15. Kwan MY, Choo A, Hanania T, Ghavami A, Beltran J, Shea J, Barboza A, Hu A, Fowler M, Neelagiri VR 2019. Biomarker Analysis of Orally Dosed, Dual Active, Matrix Metalloproteinase (MMP)-2 and MMP-9 Inhibitor, AQU-118, in the Spinal Nerve Ligation (SNL) Rat Model of Neuropathic Pain. International journal of molecular sciences 20(4):811.
16. Bonoiu A, Mahajan SD, Ye L, Kumar R, Ding H, Yong KT, Roy I, Aalinkeel R, Nair B, Reynolds JL, Sykes DE, Imperiale MA, Bergey EJ, Schwartz SA, Prasad PN 2009. MMP-9 gene silencing by a quantum dot-siRNA nanoplex delivery to maintain the integrity of the blood brain barrier. Brain Res 1282:142-155.
17. Atluri VSR, Jayant RD, Pilakka-Kanthikeel S, Garcia G, Samikkannu T, Yndart A, Kaushik A, Nair M 2016. Development of TIMP1 magnetic nanoformulation for regulation of synaptic plasticity in HIV-1 infection. International journal of nanomedicine 11:4287-4298.
18. Chaturvedi M, Molino Y, Sreedhar B, Khrestchatisky M, Kaczmarek L 2014. Tissue inhibitor of matrix metalloproteinases-1 loaded poly(lactic-co-glycolic acid) nanoparticles for delivery across the blood-brain barrier. International journal of nanomedicine 9:575-588.
19. Miyazawa T, Nakagawa K, Harigae T, Onuma R, Kimura F, Fujii T, Miyazawa T 2015. Distribution of β-carotene-encapsulated polysorbate 80-coated poly(D, L-lactide-co-glycolide) nanoparticles in rodent tissues following intravenous administration. International journal of nanomedicine 10:7223-7230.
20. Chen YH, Chang M, Davidson BL 2009. Molecular signatures of disease brain endothelia provide new sites for CNS-directed enzyme therapy. Nature medicine 15(10):1215-1218.
21. Guilfoyle MR, Carpenter KLH, Helmy A, Pickard JD, Menon DK, Hutchinson PJA 2015. Matrix Metalloproteinase Expression in Contusional Traumatic Brain Injury: A Paired Microdialysis Study. J Neurotrauma 32(20):1553-1559.
22. Lenglet S, Montecucco F, Mach F 2015. Role of matrix metalloproteinases in animal models of ischemic stroke. Curr Vasc Pharmacol 13(2):161-166.
23. Muri L, Leppert D, Grandgirard D, Leib SL 2019. MMPs and ADAMs in neurological infectious diseases and multiple sclerosis. Cellular and molecular life sciences : CMLS 76(16):3097-3116.
24. Song J, Wu C, Zhang X, Sorokin LM 2013. In vivo processing of CXCL5 (LIX) by matrix metalloproteinase (MMP)-2 and MMP-9 promotes early neutrophil recruitment in IL-1beta-induced peritonitis. Journal of immunology (Baltimore, Md : 1950) 190(1):401-410.
25. Yang Y, Rosenberg GA 2015. Matrix metalloproteinases as therapeutic targets for stroke. Brain Res 1623:30-38.
26. Brundula V, Rewcastle NB, Metz LM, Bernard CC, Yong VW 2002. Targeting leukocyte MMPs and transmigration: minocycline as a potential therapy for multiple sclerosis. Brain : a journal of neurology 125(Pt 6):1297-1308.
27. Fagan SC, Waller JL, Nichols FT, Edwards DJ, Pettigrew LC, Clark WM, Hall CE, Switzer JA, Ergul A, Hess DC 2010. Minocycline to improve neurologic outcome in stroke (MINOS): a dose-finding study. Stroke 41(10):2283-2287.
28. Metz LM, Li DKB, Traboulsee AL, Duquette P, Eliasziw M, Cerchiaro G, Greenfield J, Riddehough A, Yeung M, Kremenchutzky M, Vorobeychik G, Freedman MS, Bhan V, Blevins G, Marriott JJ, Grand'Maison F, Lee L, Thibault M, Hill MD, Yong VW 2017. Trial of Minocycline in a Clinically Isolated Syndrome of Multiple Sclerosis. N Engl J Med 376(22):2122-2133.

29. Hadass O, Tomlinson BN, Gooyit M, Chen S, Purdy JJ, Walker JM, Zhang C, Giritharan AB, Purnell W, Robinson CR, 2nd, Shin D, Schroeder VA, Suckow MA, Simonyi A, Sun GY, Mobashery S, Cui J, Chang M, Gu Z 2013. Selective inhibition of matrix metalloproteinase-9 attenuates secondary damage resulting from severe traumatic brain injury. PloS one 8(10):e76904.
30. Brown S, Bernardo MM, Li Z-H, Kotra LP, Tanaka Y, Fridman R, Mobashery S 2000. Potent and Selective Mechanism-Based Inhibition of Gelatinases. Journal of the American Chemical Society 122(28):6799-6800.
31. Koivunen E, Arap W, Valtanen H, Rainisalo A, Medina OP, Heikkila P, Kantor C, Gahmberg CG, Salo T, Konttinen YT, Sorsa T, Ruoslahti E, Pasqualini R 1999. Tumor targeting with a selective gelatinase inhibitor. Nature biotechnology 17(8):768-774.
32. Ndinguri MW, Bhowmick M, Tokmina-Roszyk D, Robichaud TK, Fields GB 2012. Peptide-based selective inhibitors of matrix metalloproteinase-mediated activities. Molecules (Basel, Switzerland) 17(12):14230-14248.
33. Bjorklund M, Heikkila P, Koivunen E 2004. Peptide inhibition of catalytic and noncatalytic activities of matrix metalloproteinase-9 blocks tumor cell migration and invasion. The Journal of biological chemistry 279(28):29589-29597.
34. Ugarte-Berzal E, Bailon E, Amigo-Jimenez I, Vituri CL, del Cerro MH, Terol MJ, Albar JP, Rivas G, Garcia-Marco JA, Garcia-Pardo A 2012. A 17-residue sequence from the matrix metalloproteinase-9 (MMP-9) hemopexin domain binds alpha4beta1 integrin and inhibits MMP-9-induced functions in chronic lymphocytic leukemia B cells. The Journal of biological chemistry 287(33):27601-27613.
35. Shimomura K, Okura T, Kato S, Couraud PO, Schermann JM, Terasaki T, Deguchi Y 2013. Functional expression of a proton-coupled organic cation (H+/OC) antiporter in human brain capillary endothelial cell line hCMEC/D3, a human blood-brain barrier model. Fluids and barriers of the CNS 10(1):8.
36. Lopalco A, Cutrignelli A, Denora N, Lopedota A, Franco M, Laquintana V 2018. Transferrin Functionalized Liposomes Loading Dopamine HCl: Development and Permeability Studies across an In Vitro Model of Human Blood-Brain Barrier. Nanomaterials (Basel, Switzerland) 8(3).
37. Liu L, Xu K, Wang H, Tan PK, Fan W, Venkatraman SS, Li L, Yang YY 2009. Self-assembled cationic peptide nanoparticles as an efficient antimicrobial agent. Nature nanotechnology 4(7):457-463.
38. Mazza M, Notman R, Anwar J, Rodger A, Hicks M, Parkinson G, McCarthy D, Daviter T, Moger J, Garrett N, Mead T, Briggs M, Schätzlein AG, Uchegbu IF 2013. Nanofiber-Based Delivery of Therapeutic Peptides to the Brain. ACS nano 7(2):1016-1026.
39. Verhoork SJM, Jennings CE, Rozatian N, Reeks J, Meng J, Corlett EK, Bunglawala F, Noble MEM, Leach AG, Coxon CR 2019. Tuning the Binding Affinity and Selectivity of Perfluoroaryl-Stapled Peptides by Cysteine-Editing. Chemistry (Easton) 25(1):177-182.
40. Heymans M, Sevin E, Gosselet F, Lundquist S, Culot M 2018. Mimicking brain tissue binding in an in vitro model of the blood-brain barrier illustrates differences between in vitro and in vivo methods for assessing the rate of brain penetration. European journal of pharmaceutics and biopharmaceutics : official journal of Arbeitsgemeinschaft fur Pharmazeutische Verfahrenstechnik eV 127:453-461.
41. Oller-Salvia B, Sanchez-Navarro M, Ciudad S, Guiu M, Arranz-Gibert P, Garcia C, Gomis RR, Cecchelli R, Garcia J, Giralt E, Teixido M 2016. MiniAp-4: A Venom-Inspired Peptidomimetic for Brain Delivery. Angewandte Chemie (International ed in English) 55(2):572-575.

42. Lee JH, Engler JA, Collawn JF, Moore BA 2001. Receptor mediated uptake of peptides that bind the human transferrin receptor. European journal of biochemistry 268(7):2004-2012.
43. Conceicao M, Mendonca L, Nobrega C, Gomes C, Costa P, Hirai H, Moreira JN, Lima MC, Manjunath N, Pereira de Almeida L 2016. Intravenous administration of brain-targeted stable nucleic acid lipid particles alleviates Machado-Joseph disease neurological phenotype. Biomaterials 82:124-137.
44. Liu Y, Li J, Shao K, Huang R, Ye L, Lou J, Jiang C 2010. A leptin derived 30-amino-acid peptide modified pegylated poly-l-lysine dendrigraft for brain targeted gene delivery. Biomaterials 31(19):5246-5257.
45. Li J, Feng L, Fan L, Zha Y, Guo L, Zhang Q, Chen J, Pang Z, Wang Y, Jiang X, Yang VC, Wen L 2011. Targeting the brain with PEG–PLGA nanoparticles modified with phage-displayed peptides. Biomaterials 32(21):4943-4950.
46. van Rooy I, Mastrobattista E, Storm G, Hennink WE, Schiffelers RM 2011. Comparison of five different targeting ligands to enhance accumulation of liposomes into the brain. J Controlled Release 150(1):30-36.
47. Somani S, Robb G, Pickard BS, Dufès C 2015. Enhanced gene expression in the brain following intravenous administration of lactoferrin-bearing polypropylenimine dendriplex. J Controlled Release 217:235-242.
48. Deng G, Zhou F, Wu Z, Zhang F, Niu K, Kang Y, Liu X, Wang Q, Wang Y, Wang Q 2017. Inhibition of cancer cell migration with CuS@ mSiO(2)-PEG nanoparticles by repressing MMP-2/MMP-9 expression. International journal of nanomedicine 13:103-116.
49. Liu X, Ren Q, Fu F, Zou R, Wang Q, Xin G, Xiao Z, Huang X, Liu Q, Hu J 2015. CuS@mSiO2-PEG core–shell nanoparticles as a NIR light responsive drug delivery nanoplatform for efficient chemo-photothermal therapy. Dalton Transactions 44(22):10343-10351.
50. Muldoon LL, Pagel MA, Kroll RA, Roman-Goldstein S, Jones RS, Neuwelt EA 1999. A physiological barrier distal to the anatomic blood-brain barrier in a model of transvascular delivery. AJNR American journal of neuroradiology 20(2):217-222.
51. Trentini A, Castellazzi M, Cervellati C, Manfrinato MC, Tamborino C, Hanau S, Volta CA, Baldi E, Kostic V, Drulovic J, Granieri E, Dallocchio F, Bellini T, Dujmovic I, Fainardi E 2016. Interplay between Matrix Metalloproteinase-9, Matrix Metalloproteinase-2, and Interleukins in Multiple Sclerosis Patients. Disease markers 2016:3672353.
52. Torrecilla J, Gomez-Aguado I, Vicente-Pascual M, Del Pozo-Rodriguez A, Solinis MA, Rodriguez-Gascon A 2019. MMP-9 Downregulation with Lipid Nanoparticles for Inhibiting Corneal Neovascularization by Gene Silencing. Nanomaterials (Basel, Switzerland) 9(4).
53. Hashimoto M, Sasaki JI, Yamaguchi S, Kawai K, Kawakami H, Iwasaki Y, Imazato S 2015. Gold Nanoparticles Inhibit Matrix Metalloproteases without Cytotoxicity. Journal of dental research 94(8):1085-1091.
54. Hutter E, Boridy S, Labrecque S, Lalancette-Hébert M, Kriz J, Winnik FM, Maysinger D 2010. Microglial Response to Gold Nanoparticles. ACS nano 4(5):2595-2606.
55. Akram MW, Fakhar-e-Alam M, Atif M, Butt AR, Asghar A, Jamil Y, Alimgeer KS, Wang ZM 2018. In vitro evaluation of the toxic effects of MgO nanostructure in Hela cell line. Sci Rep 8(1):4576.
56. Weidner M, Hüwel S, Ebert F, Schwerdtle T, Galla H-J, Humpf H-U 2013. Influence of T-2 and HT-2 toxin on the blood-brain barrier in vitro: new experimental hints for neurotoxic effects. PloS one 8(3):e60484-e60484.

57. Fatouros DG, Lamprou DA, Urquhart AJ, Yannopoulos SN, Vizirianakis IS, Zhang S, Koutsopoulos S 2014. Lipid-like Self-Assembling Peptide Nanovesicles for Drug Delivery. ACS Applied Materials & Interfaces 6(11):8184-8189.
58. Jeong W-j, Lim Y-b 2014. Macrocyclic Peptides Self-Assemble into Robust Vesicles with Molecular Recognition Capabilities. Bioconjugate Chem 25(11):1996-2003.
59. Gudlur S, Sukthankar P, Gao J, Avila LA, Hiromasa Y, Chen J, Iwamoto T, Tomich JM 2012. Peptide Nanovesicles Formed by the Self-Assembly of Branched Amphiphilic Peptides. PloS one 7(9):e45374.
60. Holowka EP, Sun VZ, Kamei DT, Deming TJ 2007. Polyarginine segments in block copolypeptides drive both vesicular assembly and intracellular delivery. Nature materials 6(1):52-57.
61. Rodríguez-Hernández J, Lecommandoux S 2005. Reversible Inside−Out Micellization of pH-responsive and Water-Soluble Vesicles Based on Polypeptide Diblock Copolymers. Journal of the American Chemical Society 127(7):2026-2027.
62. van Hell AJ, Costa CI, Flesch FM, Sutter M, Jiskoot W, Crommelin DJ, Hennink WE, Mastrobattista E 2007. Self-assembly of recombinant amphiphilic oligopeptides into vesicles. Biomacromolecules 8(9):2753-2761.
63. Holowka EP, Pochan DJ, Deming TJ 2005. Charged Polypeptide Vesicles with Controllable Diameter. Journal of the American Chemical Society 127(35):12423-12428.
64. Wu L-P, Ahmadvand D, Su J, Hall A, Tan X, Farhangrazi ZS, Moghimi SM 2019. Crossing the blood-brain-barrier with nanoligand drug carriers self-assembled from a phage display peptide. Nature communications 10(1):4635.
65. Biemans EALM, Jäkel L, de Waal RMW, Kuiperij HB, Verbeek MM 2017. Limitations of the hCMEC/D3 cell line as a model for Aβ clearance by the human blood-brain barrier. J Neurosci Res 95(7):1513-1522.
66. Campisi M, Shin Y, Osaki T, Hajal C, Chiono V, Kamm RD 2018. 3D self-organized microvascular model of the human blood-brain barrier with endothelial cells, pericytes and astrocytes. Biomaterials 180:117-129.
67. Siddharthan V, Kim YV, Liu S, Kim KS 2007. Human astrocytes/astrocyte-conditioned medium and shear stress enhance the barrier properties of human brain microvascular endothelial cells. Brain Research 1147:39-50.
68. Bagchi S, Chhibber T, Lahooti B, Verma A, Borse V, Jayant RD 2019. In-vitro blood-brain barrier models for drug screening and permeation studies: an overview. Drug Des Devel Ther 13:3591-3605.
69. Khongkow M, Yata T, Boonrungsiman S, Ruktanonchai UR, Graham D, Namdee K 2019. Surface modification of gold nanoparticles with neuron-targeted exosome for enhanced blood–brain barrier penetration. Sci Rep 9(1):8278.
70. Gynther M, Laine K, Ropponen J, Leppanen J, Mannila A, Nevalainen T, Savolainen J, Jarvinen T, Rautio J 2008. Large neutral amino acid transporter enables brain drug delivery via prodrugs. Journal of medicinal chemistry 51(4):932-936.
71. Chaturvedi M, Kaczmarek L 2014. MMP-9 Inhibition: a Therapeutic Strategy in Ischemic Stroke. Mol Neurobiol 49(1):563-573.
72. Wang Y, Luo J, Li SY 2019. Nano-Curcumin Simultaneously Protects the Blood-Brain Barrier and Reduces M1 Microglial Activation During Cerebral Ischemia-Reperfusion Injury. ACS Appl Mater Interfaces 11(4):3763-3770.
73. Kassner A, Merali Z 2015. Assessment of Blood-Brain Barrier Disruption in Stroke. Stroke 46(11):3310-3315.
74. Panahpour H, Farhoudi M, Omidi Y, Mahmoudi J 2018. An In Vivo Assessment of Blood-Brain Barrier Disruption in a Rat Model of Ischemic Stroke. J Vis Exp (133).

75. Bao Q, Hu P, Xu Y, Cheng T, Wei C, Pan L, Shi J 2018. Simultaneous Blood-Brain Barrier Crossing and Protection for Stroke Treatment Based on Edaravone-Loaded Ceria Nanoparticles. ACS nano 12(7):6794-6805.
76. Setyopranoto I, Malueka RG, Panggabean AS, Widyadharma IPE, Sadewa AH, Lamsudin R, Wibowo S 2018. Association between Increased Matrix Metalloproteinase-9 (MMP-9) Levels with Hyperglycaemia Incidence in Acute Ischemic Stroke Patients. Open access Macedonian journal of medical sciences 6(11):2067-2072.
77. Bhowmick M, Tokmina-Roszyk D, Onwuha-Ekpete L, Harmon K, Robichaud T, Fuerst R, Stawikowska R, Steffensen B, Roush W, Wong HR, Fields GB 2017. Second Generation Triple-Helical Peptide Inhibitors of Matrix Metalloproteinases. J Med Chem 60(9):3814-3827.
78. Scannevin RH, Alexander R, Haarlander TM, Burke SL, Singer M, Huo C, Zhang YM, Maguire D, Spurlino J, Deckman I, Carroll KI, Lewandowski F, Devine E, Dzordzorme K, Tounge B, Milligan C, Bayoumy S, Williams R, Schalk-Hihi C, Leonard K, Jackson P, Todd M, Kuo LC, Rhodes KJ 2017. Discovery of a highly selective chemical inhibitor of matrix metalloproteinase-9 (MMP-9) that allosterically inhibits zymogen activation. The Journal of biological chemistry 292(43):17963-17974.

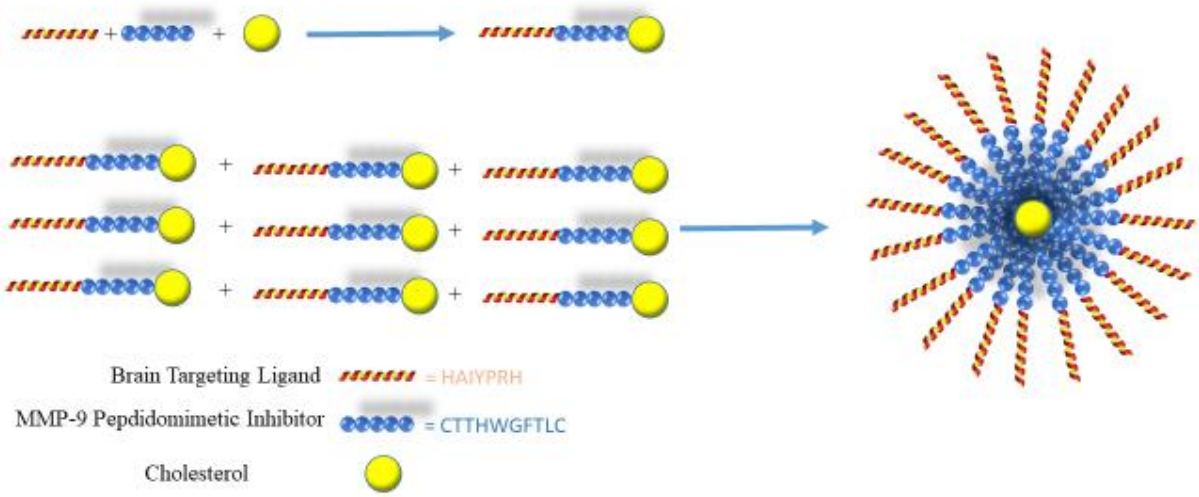

Figure 1: A) Schematic diagram of the formation of self-assembled MMP-9 inhibiting NPs by amphiphilic peptides.

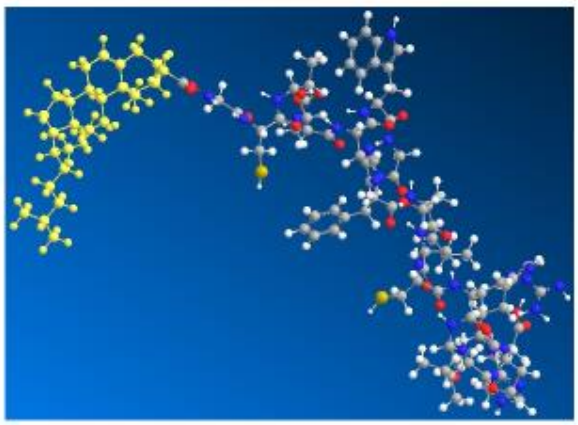

Figure 1: B) Ball and stick presentation of the MMP-9 inhibiting amphiphilic compound: Cholesterol-CTTHWGFTLCHAIYPRH. Cholesterol is presented as yellow ball and sticks.

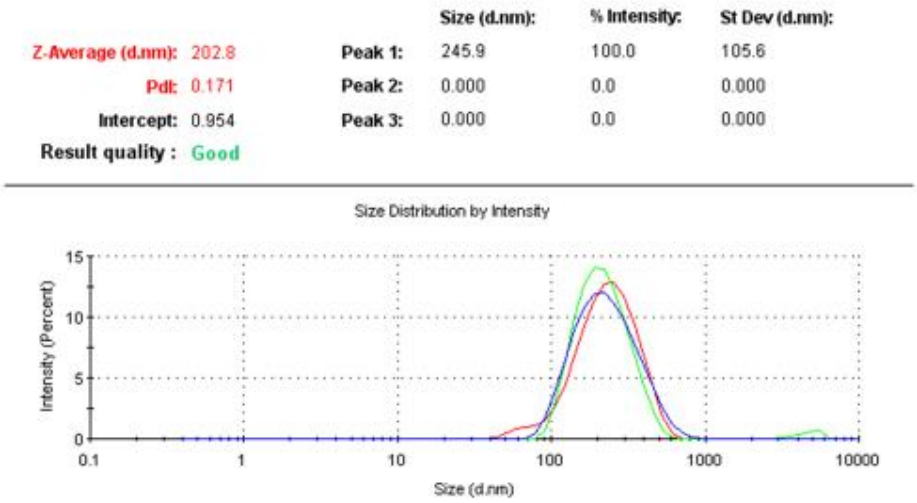

Figure 2: Particle size distribution report of MMP-9 inhibiting nanoparticles obtained by the DLS method. This figure shows three different measurements. The average particle size and PdI are presented at the top of figure.

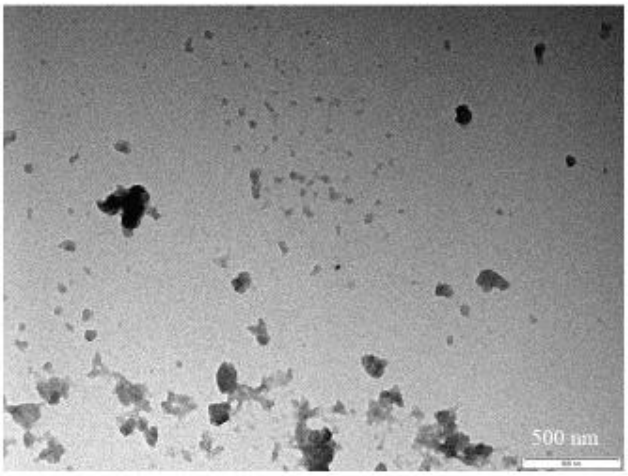

Figure 3: TEM images of MMP-9 inhibiting NPs, presenting irregular shape of NPs. The scale bar is 500 nm.

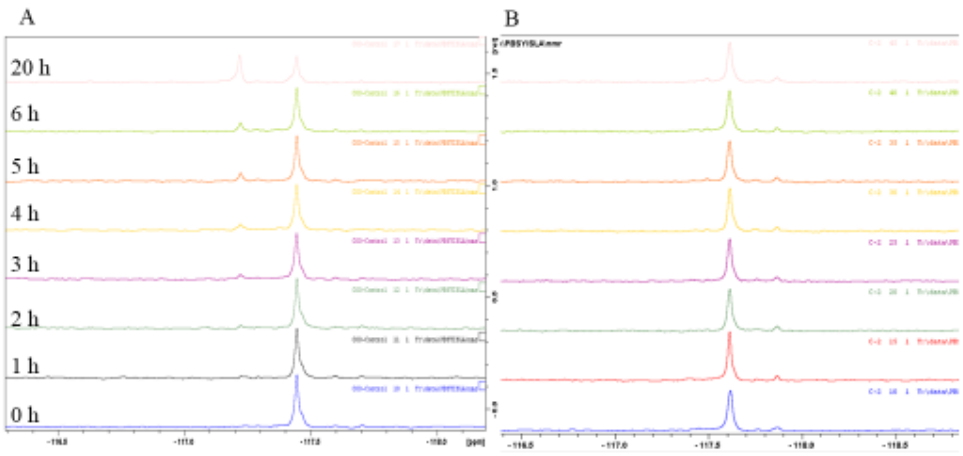

Figure 4: ^{19}F NMR data presenting the inhibition of MMP-9 by MMP-9 inhibiting NPs. A) Cleavage of a MMP-9 cleavable peptide (TY-26) by MMP-9 enzyme is represented by disappearing signal at -117.5 ppm and appearance of enzyme degradation product signal at -117.2 ppm, B) The inhibition of TY-26 cleavage by MMP-9 inhibiting NPs in the presence of MMP-9 enzyme is shown by persistent signal at -117.6 ppm and no any other signals.

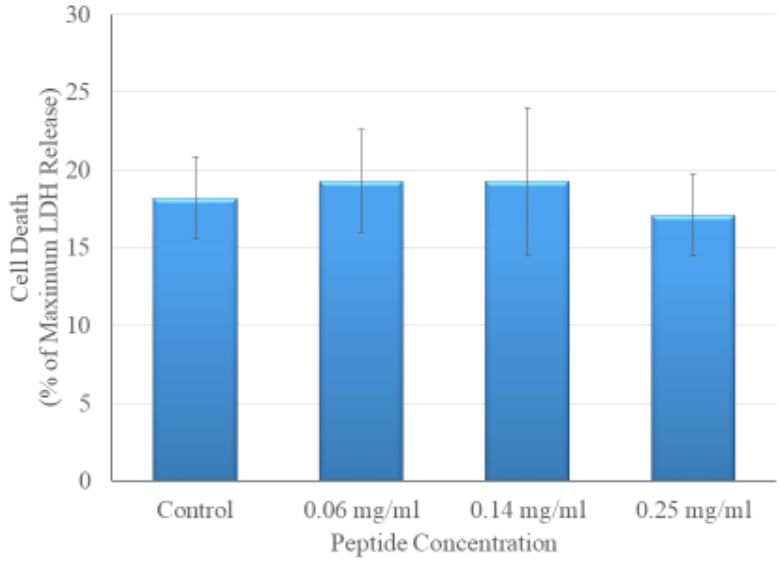

Figure 5: Cell toxicity of MMP-9 inhibiting NPs towards HeLa cells measured by LDH release. Lack of toxicity of MMP-9 inhibiting NPs is indicated by LDH release comparable to control tests. LDH release is expressed as mean ± SD (n=3).

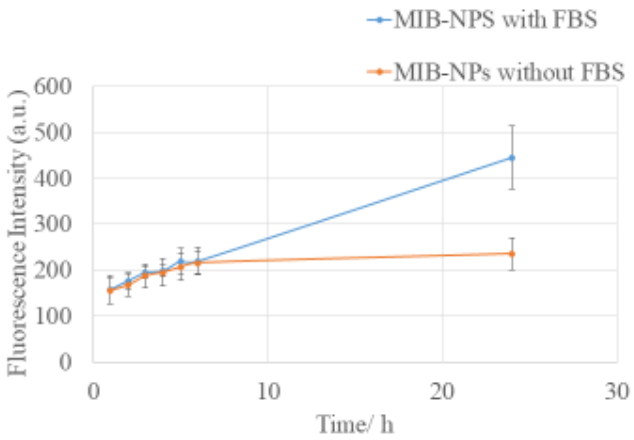

Figure 6: Release of MMP-9 inhibiting NPs (MIB-NPs) from a dialysis bag with or without the presence of foetal bovine serum (FBS), presenting degradation of MIB-NPs by enzymes in the FBS and slight disintegrations of MIB-NPs upon dilution. Error bars present SD (n=3).

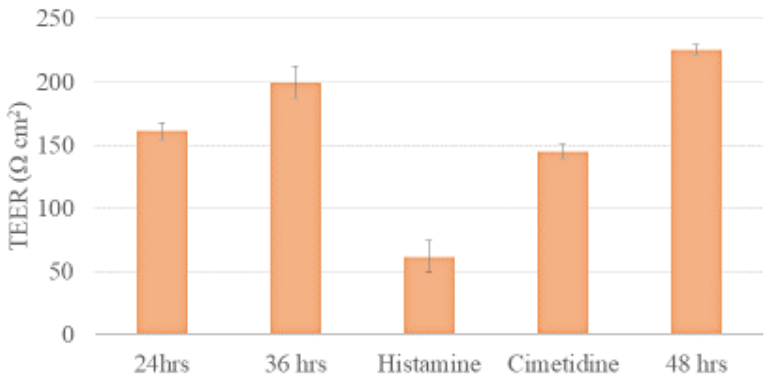

Figure 7: TEER values for *in vitro* BBB prepared by hCMEC/D3 cells seeded at 90000/insert after 24 h, 36 h, post histamine and post cimetidine treatment, presenting formation of a biological barrier that can be compromised by pharmacological compounds (histamine) and restated by pharmacological agents (cimetidine). Error bar indicate SD (n=3).

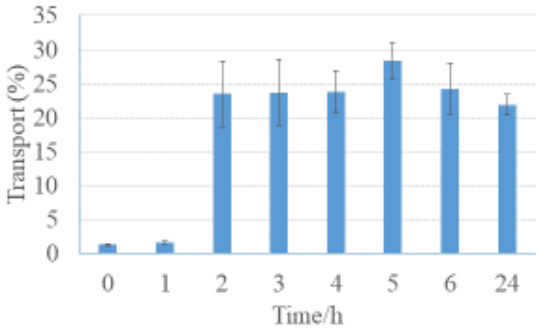

Figure 8: Transmigration study of MMP-9 inhibiting NPs using hCMEC/D3 *in vitro* BBB model, demonstrating ability of the NPs to cross the BBB after 2 h incubation at 37°C. Also, the figure presents gradual drop in transmigrated NPs to the basolateral compartment after 5 h incubation. Error bars present SD (n=3).

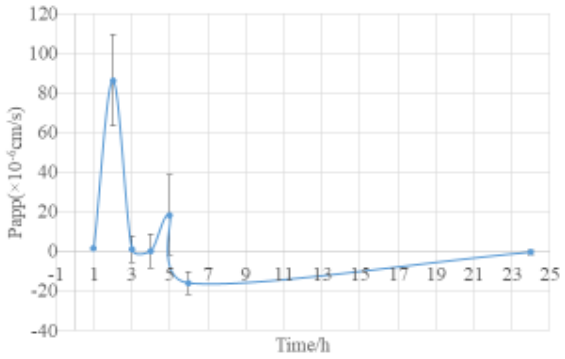

Figure 9: The relationship between *in vitro* brain permeability and time for MMP-9 inhibiting NPs using hCMEC/D3 cell line. It can be seen that Papp reduced considerably after 2 hr incubation and it was negative after 5 hr incubation. This observation suggests reverse of NPs from the basolateral compartment to the apical compartment. Error bars present SD (n=3).

Figure S1. HPLC DATA for Peptide 1

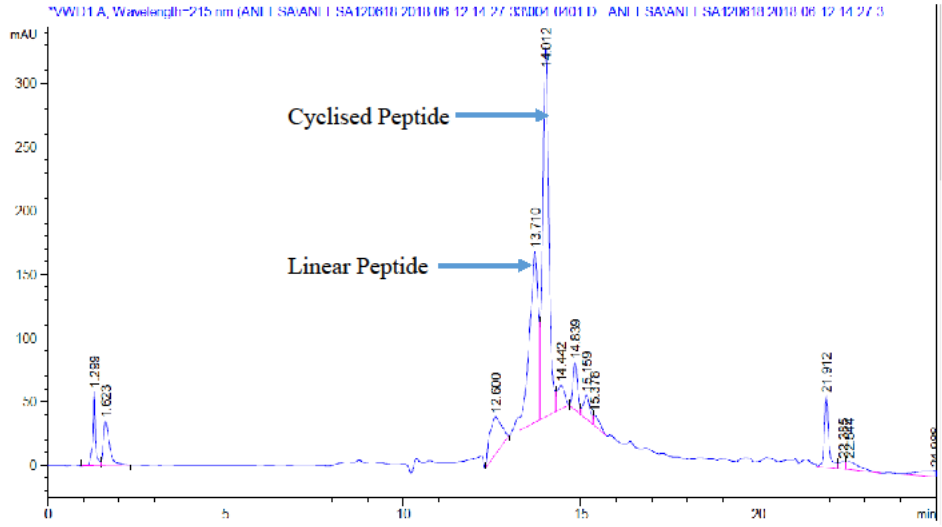

Figure S2: HPLC Data for Peptide 2

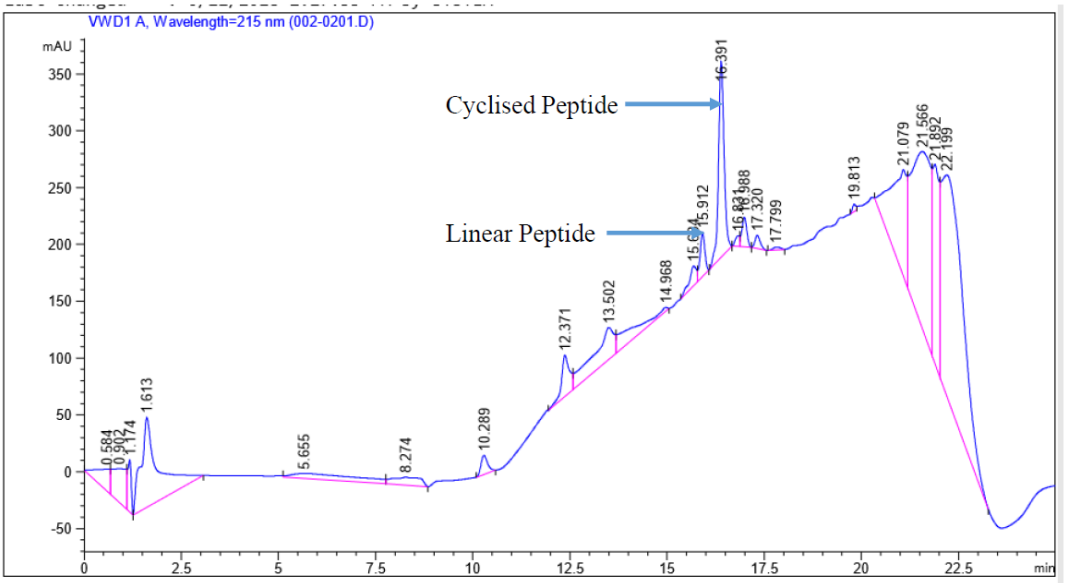

Figure S3. HPLC DATA for Peptide 3

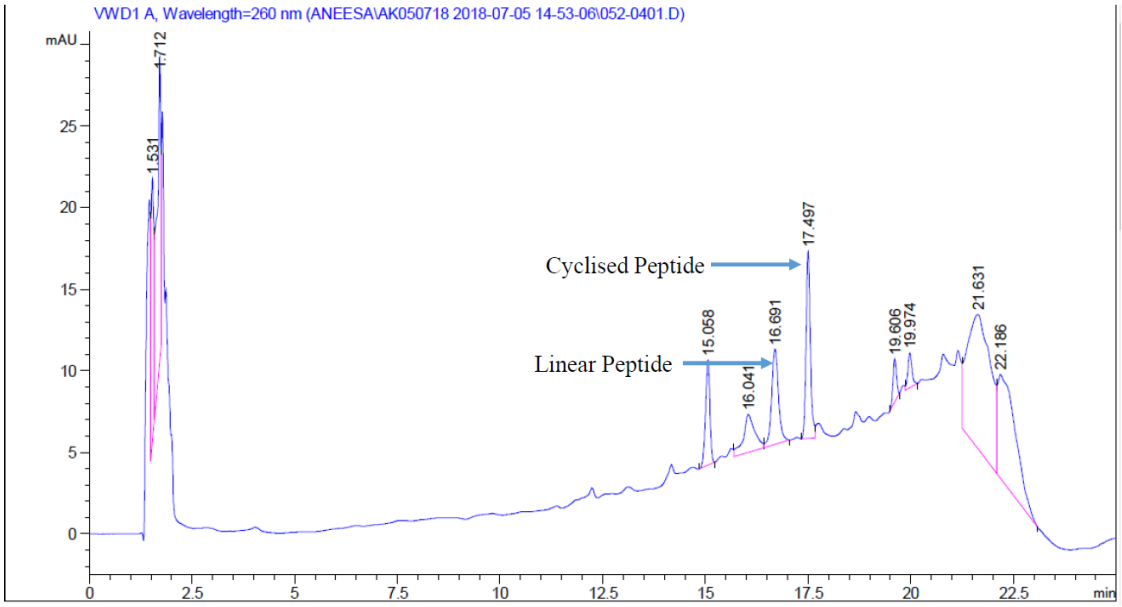

Figure S4. LC/MS for Peptide 3

Figure S5. LC/MS Spectrum for conjugated Peptide 3

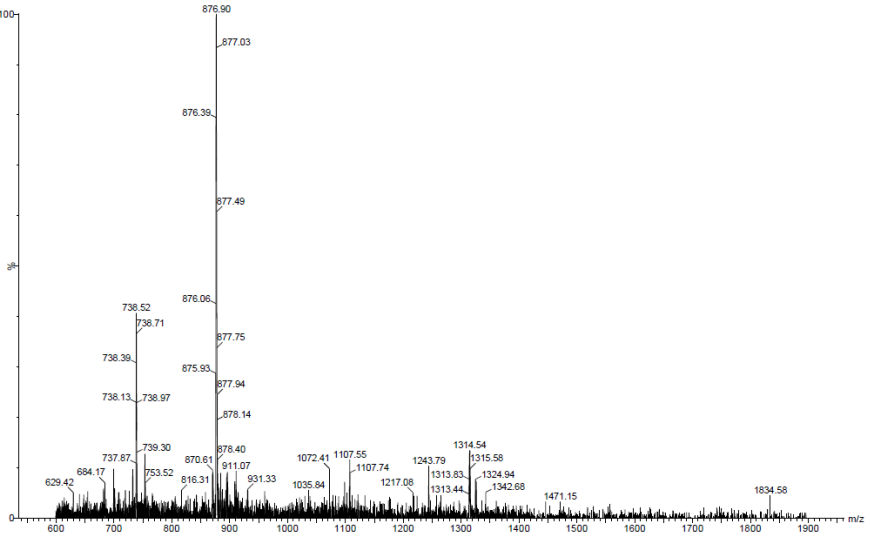

Figure S6: UV chromatogram for Conjugated Peptide 3.

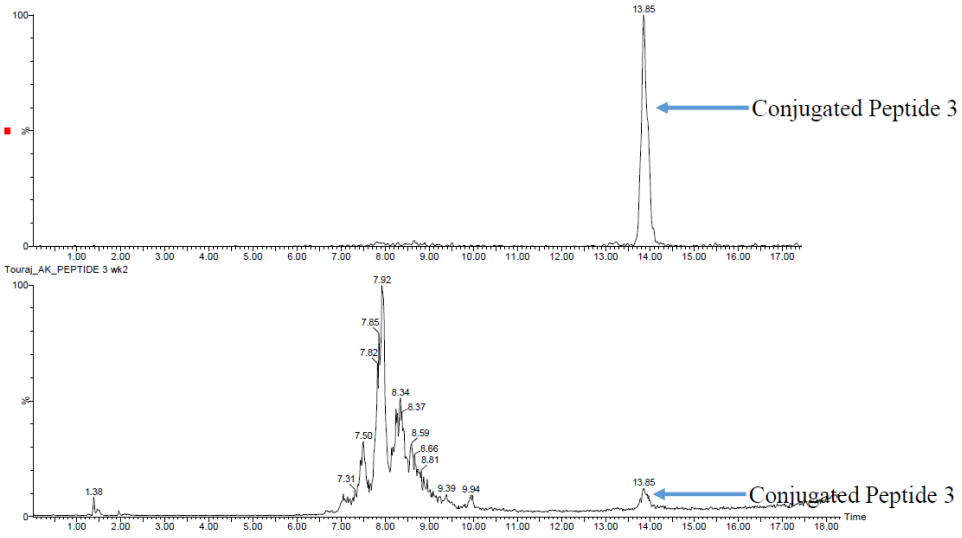

Figure S7. NMR DATA for duplicate run of TY-26 in the presence of MMP-9 enzyme

$K_{Metabolite}=4.54x10^{-06}$

Figure S7a

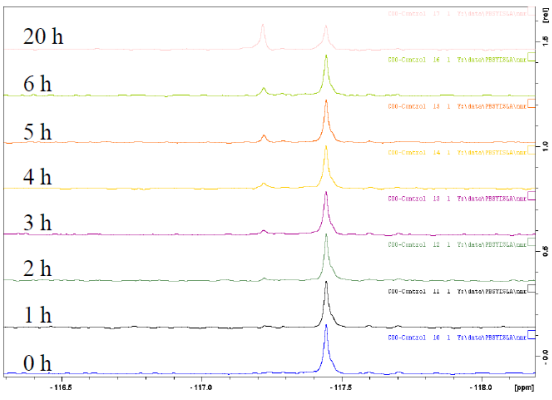

Control

$K_{Metabolite}=1.92x10^{-6}$

Figure S7b

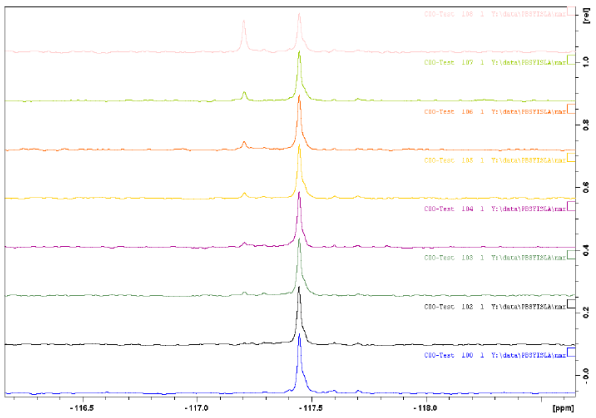

With MMP-9 Inhibiting Nanocarriers

Figure S8: NMR DATA for TY-26 in TCNB Buffer only for 14 h

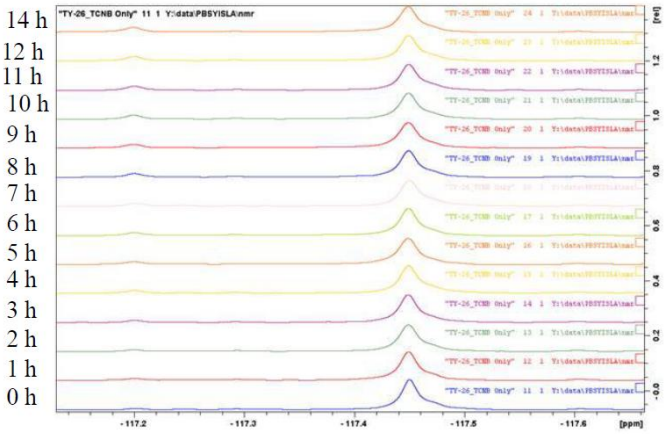

Figure S9: TY-27 (GGYGQ-GYW^{19}FG) a negative control after 14 h in the presence of MMP-9

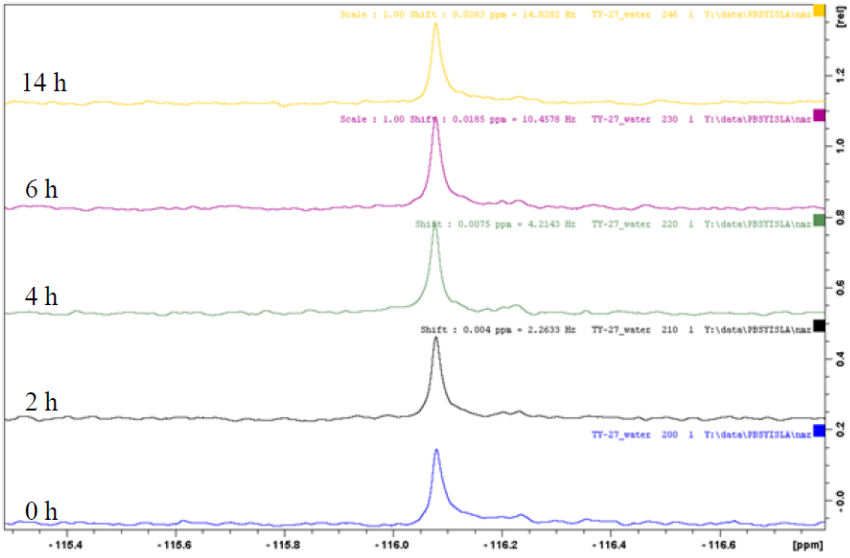

Figure S10, typical fluorescence curve obtained in dialysis studies